JOURNAL OF THERMOPHYSICS AND HEAT TRANSFER
Vol. 7, No. 4, Oct.–Dec. 1993

Three-Dimensional Upwind Parabolized Navier-Stokes Code for Supersonic Combustion Flowfields

Ganesh Wadawadigi,* John C. Tannehill,† and Philip E. Buelow‡
Iowa State University, Ames, Iowa 50011
and
Scott L. Lawrence§
NASA Ames Research Center, Moffett Field, California 94035

A new upwind, parabolized Navier-Stokes (PNS) code has been developed to compute the three-dimensional chemically reacting flow in scramjet (supersonic combustion ramjet) engines. The code is a modification of the three-dimensional upwind PNS (UPS) airflow code which has been extended in the present study to permit internal flow calculations with hydrogen-air chemistry. With these additions, the new code has the capability of computing both aerodynamic and propulsive flowfields. The algorithm solves the PNS equations using a finite-volume, upwind TVD method based on Roe's approximate Riemann solver that has been modified to account for nonequilibrium effects. The fluid medium is assumed to be a chemically reacting mixture of thermally perfect (but calorically imperfect) gases in thermal equilibrium. The new code has been applied to two test cases. These include the Burrows-Kurkov supersonic combustion experiment and a three-dimensional shock-induced combustion flowfield. The computed results compare favorably with the available experimental data.

Introduction

THE design of hypersonic vehicles such as the National Aero-Space Plane (NASP) requires the accurate calculation of both external and internal hypersonic flows. The NASP utilizes a scramjet propulsion system which is integrated with the aerodynamics on the underside of the vehicle. The forebody of the NASP acts as a compression region for the scramjet, while the aftbody serves as part of the nozzle. As a consequence, the aerodynamic and propulsive flowfields must be computed concurrently.

The numerical simulation of both external and internal hypersonic flows with finite-rate chemistry has evolved rapidly in the last few years. Numerous numerical methods have been proposed that either solve the unsteady Navier-Stokes (NS) equations[1–11] or the steady parabolized Navier-Stokes (PNS) equations.[8,12–27] The unsteady NS solvers are required if the inviscid portion of the flow becomes subsonic, such as in the nose region of a blunt vehicle. Aft of the nose region, the flow can be more efficiently solved using a PNS code if the inviscid portion of the flow remains supersonic and if there is no streamwise flow separation.

Lawrence et al.[28,29] have developed a robust upwind (perfect gas) PNS code (UPS code) which solves the PNS equations using a finite-volume, upwind TVD method based on Roe's approximate Riemann solver.[30] The dissipation term associated with this scheme is sufficiently adaptive to various flow conditions so that no user-specified smoothing is required. This eliminates the problem of determining the correct amount of smoothing which "plagued" many of the previous centrally-differenced PNS codes. The two-dimensional[28] and three-dimensional[29] versions of the UPS code have been extended to permit both equilibrium[19,25] and nonequilibrium[20,27] (finite-rate chemically reacting) airflow computations. For nonequilibrium flows, the fluid dynamic and species continuity equations are solved in a loosely-coupled manner. The coupling can be enhanced with an iterative procedure if necessary. An advantage of the loosely-coupled approach is that as the complexity of the chemistry model increases, only the chemistry solution is affected and the solution procedure for the fluids remains essentially unaltered. Another advantage is that the system of equations for the chemistry can be solved without the need for block inversions which are computationally expensive.

In the present work, the three-dimensional UPS code has been further extended to permit internal turbulent flow calculations with hydrogen-air chemistry. The chemistry model contains 11 reactions and 9 species and is based on the NASP model.[31] With these additions, the new code has the capability of computing both aerodynamic and propulsive flowfields. The code has been applied to two internal flow test cases. The first case consists of the Burrows-Kurkov supersonic combustion experiment[32] in which hydrogen was injected tangentially at sonic speed through a slot in the floor of a test section with a $M_\infty = 2.44$ vitiated airstream. In the second test case, the code is used to compute a three-dimensional ($M_\infty = 7.0$) shock-induced combustion flowfield. The computed results are compared with experimental data wherever possible.

Governing Equations

The PNS equations are used in the present study to model the fluid dynamics. These are obtained from the steady, compressible Navier-Stokes equations by neglecting streamwise viscous terms and by retaining only a fraction of the streamwise pressure gradient term in the subsonic layer in order to eliminate ellipticity in the marching direction. The latter is accomplished using Vigneron's technique[33] in conjunction with the extension to chemically reacting flows by Prabhu et al.[15]

Presented as Paper 92-2898 at the AIAA 27th Thermophysics Conference, Nashville, TN, July 6–8, 1992; received July 17, 1992; revision received Nov. 5, 1992; accepted for publication Dec. 15, 1992.

*Graduate Research Assistant, Department of Aerospace Engineering and Engineering Mechanics. Student Member AIAA.

†Manager, Computational Fluid Dynamics Center and Professor, Department of Aerospace Engineering and Engineering Mechanics. Associate Fellow AIAA.

‡Graduate Research Assistant, Department of Aerospace Engineering and Engineering Mechanics; currently at Pennsylvania State University, University Park, PA 16802. Member AIAA.

§Research Scientist, Applied Computational Fluid Dynamics Branch. Member AIAA.

The PNS equations expressed in generalized coordinates (ξ, η, ζ) are given by

$$\boldsymbol{E}_\xi + \boldsymbol{F}_\eta + \boldsymbol{G}_\zeta = 0 \tag{1}$$

where

$$\begin{aligned} \boldsymbol{E} &= (\xi_x/J)\boldsymbol{E}_i + (\xi_y/J)\boldsymbol{F}_i + (\xi_z/J)\boldsymbol{G}_i \\ \boldsymbol{F} &= (\eta_x/J)(\boldsymbol{E}_i - \boldsymbol{E}_v^*) + (\eta_y/J)(\boldsymbol{F}_i - \boldsymbol{F}_v^*) \\ &\quad + (\eta_z/J)(\boldsymbol{G}_i - \boldsymbol{G}_v^*) \\ \boldsymbol{G} &= (\zeta_x/J)(\boldsymbol{E}_i - \boldsymbol{E}_v^*) + (\zeta_y/J)(\boldsymbol{F}_i - \boldsymbol{F}_v^*) \\ &\quad + (\zeta_z/J)(\boldsymbol{G}_i - \boldsymbol{G}_v^*) \end{aligned} \tag{2}$$

The inviscid and viscous flux vectors are given by

$$\begin{aligned} \boldsymbol{E}_i &= [\rho u, \rho u^2 + p, \rho uv, \rho uw, (E_t + p)u]^T \\ \boldsymbol{F}_i &= [\rho v, \rho uv, \rho v^2 + p, \rho vw, (E_t + p)v]^T \\ \boldsymbol{G}_i &= [\rho w, \rho uw, \rho vw, \rho w^2 + p, (E_t + p)w]^T \\ \boldsymbol{E}_v &= (0, \tau_{xx}, \tau_{xy}, \tau_{xz}, u\tau_{xx} + v\tau_{xy} + w\tau_{xz} - q_x)^T \\ \boldsymbol{F}_v &= (0, \tau_{yx}, \tau_{yy}, \tau_{yz}, u\tau_{yx} + v\tau_{yy} + w\tau_{yz} - q_y)^T \\ \boldsymbol{G}_v &= (0, \tau_{zx}, \tau_{zy}, \tau_{zz}, u\tau_{zx} + v\tau_{zy} + w\tau_{zz} - q_z)^T \end{aligned} \tag{3}$$

where $E_t = \rho[e + \frac{1}{2}(u^2 + v^2 + w^2)]$.

The effect of mass diffusion of the species is accounted for by adding the following component to the heat flux terms (q_x, q_y, q_z):

$$\rho \sum_{s=1}^{n} c_s \boldsymbol{U}_s h_s \tag{4}$$

where $\boldsymbol{U}_s$ is the diffusion velocity of species s, c_s is the species mass fraction, and h_s is the species enthalpy. The superscript asterisks on the viscous flux vectors in Eq. (2) indicate that the derivatives with respect to ξ have been dropped. In the above equations, p is the pressure; ρ is the density; u, v, and w are the velocity components in the x, y, and z directions, respectively; e is the internal energy; τ is the viscous stress; and q is the heat conduction rate. The dependent variables have been nondimensionalized as follows:

$$\begin{aligned} x, y, z &= \frac{x^*, y^*, z^*}{L^*} & u, v, w &= \frac{u^*, v^*, w^*}{V_\infty^*} \\ e &= \frac{e^*}{V_\infty^{*2}} & p &= \frac{p^*}{\rho_\infty^* V_\infty^{*2}} \\ \mu &= \frac{\mu^*}{\mu_\infty^*} & \rho &= \frac{\rho^*}{\rho_\infty^*} \\ \kappa &= \frac{\kappa^*}{\kappa_\infty^*} & T &= \frac{T^*}{T_\infty^*} \end{aligned}$$

The species continuity equation is given by

$$\frac{\partial \rho_s}{\partial t} + \nabla \cdot (\rho_s \boldsymbol{V}_s) = \dot{\omega}_s, \qquad s = 1, 2, \ldots, n \tag{5}$$

where $\boldsymbol{V}_s$ is the sum of the fluid velocity $\boldsymbol{V}$ and the species diffusion velocity $\boldsymbol{U}_s$. The species density is denoted by ρ_s and the term $\dot{\omega}_s$ is the mass production or depletion rate of the species s which is a function of the temperature, density, and the mass concentration of the reactants constituting the mixture. The subscript s denotes the species index. Using the global continuity equation and assuming Fick's law for mass diffusion, the above form of the species continuity equation is simplified to

$$\rho \left[\frac{\partial c_s}{\partial t} + \boldsymbol{V} \cdot \nabla c_s \right] = \nabla \cdot (\beta_3 \rho \mathcal{D}_{sm} \nabla c_s) + \dot{\omega}_s \tag{6}$$

where the nondimensional quantity β_3 is

$$\beta_3 = \frac{\rho_\infty^* \mathcal{D}_\infty^*}{\mu_\infty^* Re_\infty}$$

and $\mathcal{D}_{sm}$ is the multicomponent diffusion coefficient for the species s. In the present work, a kinetic binary diffusion coefficient $\mathcal{D}$ is used and assumed to be the same for all the species. The species continuity equation is simplified using the PNS approximation of dropping the unsteady term and neglecting the streamwise diffusion terms. After recasting the equation into generalized coordinates, the final form is obtained

$$\begin{aligned} &\rho \hat{U} \frac{\partial c_s}{\partial \xi} + \rho \hat{V} \frac{\partial c_s}{\partial \eta} + \rho \hat{W} \frac{\partial c_s}{\partial \zeta} - \frac{\partial}{\partial \eta} \left[A_{\eta\eta} \frac{\partial c_s}{\partial \eta} + A_{\eta\zeta} \frac{\partial c_s}{\partial \zeta} \right] \\ &\quad - \frac{\partial}{\partial \zeta} \left[A_{\zeta\zeta} \frac{\partial c_s}{\partial \zeta} + A_{\zeta\eta} \frac{\partial c_s}{\partial \eta} \right] = \frac{\dot{\omega}_s}{J} \end{aligned} \tag{7}$$

where

$$\begin{aligned} \hat{U} &= (\xi_x/J)u + (\xi_y/J)v + (\xi_z/J)w \\ \hat{V} &= (\eta_x/J)u + (\eta_y/J)\, v + (\eta_z/J)w \\ \hat{W} &= (\zeta_x/J)u + (\zeta_y/J)v + (\zeta_z/J)w \end{aligned} \tag{8}$$

$$\begin{aligned} A_{\eta\eta} &= \beta_3 \rho \mathcal{D} \left[\frac{\eta_x^2}{J} + \frac{\eta_y^2}{J} + \frac{\eta_z^2}{J} \right] \\ A_{\zeta\zeta} &= \beta_3 \rho \mathcal{D} \left[\frac{\zeta_x^2}{J} + \frac{\zeta_y^2}{J} + \frac{\zeta_z^2}{J} \right] \\ A_{\eta\zeta} = A_{\zeta\eta} &= \beta_3 \rho \mathcal{D} \left[\frac{\eta_x \zeta_x}{J} + \frac{\eta_y \zeta_y}{J} + \frac{\eta_z \zeta_z}{J} \right] \end{aligned} \tag{9}$$

In addition to the above equations, the equation of state is used

$$p = (\beta_1 \rho T / \mathcal{M}) \tag{10}$$

where the nondimensional quantity β_1 and molecular weight of the mixture $\mathcal{M}$ are given by

$$\beta_1 = \frac{\mathcal{R}_U^* T_\infty^*}{\mathcal{M}_\infty^* V_\infty^{*2}}, \qquad \mathcal{M} = \left(\sum_{s=1}^{n} \frac{c_s}{\mathcal{M}_s} \right)^{-1}$$

and $\mathcal{R}_U$ is the universal gas constant (8314.34 J/kmole/K). The ratio of sensible enthalpy and sensible energy is defined as $\bar{\gamma}$ where the sensible energy (e^s) is expressed in terms of the species mass fractions (c_s) and the species formation enthalpy at 0 K (h_{fs}^0) by

$$e^s = e - \sum_{s=1}^{n} c_s h_{fs}^0$$

In addition, the following nondimensional quantities are used:

$$\begin{aligned} \mathcal{M} &= \frac{\mathcal{M}^*}{\mathcal{M}_\infty} & C_{pf} &= \frac{C_{pf}^* T_\infty^*}{V_\infty^{*2}} \\ \dot{\omega}_s^* &= \frac{\dot{\omega}_s^*}{\rho_\infty^* V_\infty^*} & \mathcal{D} &= \frac{\mathcal{D}^*}{\mathcal{D}_\infty^*} \end{aligned}$$

Thermodynamic and Transport Properties

Enthalpy and Specific Heat

The enthalpies and specific heats are obtained from a table lookup procedure using the data of Ref. 34. Cubic spline interpolation is used to find the property at a particular temperature. Since the enthalpies in Ref. 34 are referenced to 298.15 K, they are re-referenced to 0 K in the following manner. For each species, the enthalpy at 0 K is subtracted from the enthalpy at a particular temperature T (all referenced to 298.15 K). This yields the sensible enthalpy referenced to 0 K at the temperature T. The species formation enthalpy at 0 K is then added to obtain the properly referenced enthalpy. The enthalpy and frozen specific heat of the mixture are given by

$$\begin{gathered} h^* = \sum_{s=1}^{n} c_s h_s^* \\ C_{pf}^* = \left.\frac{dh^*}{dT^*}\right|_{c_1,\ldots,c_n} = \sum_{s=1}^{n} c_s \frac{dh_s^*}{dT^*} = \sum_{s=1}^{n} c_s C_{p,s}^* \end{gathered} \tag{11}$$

where the subscripts on the differentiation denote that the mixture composition is locally frozen.

Viscosity and Thermal Conductivity

Cubic spline interpolation is employed to obtain the species viscosity (μ_s) from the tabulated data given in Ref. 35. The thermal conductivity of species s is computed using Eucken's semiempirical formula

$$\kappa_s^* = \frac{\mu_s^* \mathcal{R}^*}{\mathcal{M}_s^*}\left(C_{p,s}^* \frac{\mathcal{M}_s^*}{\mathcal{R}^*} + \frac{5}{4}\right)$$

The viscosity and thermal conductivity of the mixture are calculated using Wilke's semiempirical mixing rule[36]

$$\mu^* = \sum_{s=1}^{n} \frac{X_s \mu_s^*}{\phi_s}, \qquad \kappa^* = \sum_{s=1}^{n} \frac{X_s \kappa_s^*}{\phi_s} \tag{12}$$

where

$$X_s = \frac{c_s \mathcal{M}^*}{\mathcal{M}_s^*}$$

$$\phi_s = \sum_{r=1}^{n} X_r \left[1 + \sqrt{\frac{\mu_s^*}{\mu_r^*}} \left(\frac{\mathcal{M}_r^*}{\mathcal{M}_s^*}\right)^{1/4}\right]^2 \left[\sqrt{8}\sqrt{1 + \frac{\mathcal{M}_r^*}{\mathcal{M}_s^*}}\right]^{-1}$$

Diffusion Coefficient

The binary Lewis number $\mathcal{L}e$ is assumed to be the same constant for all the species and is taken to be unity[37] for the present calculations. The kinematic diffusion coefficient $\mathcal{D}^*$ is then computed from the definition

$$\mathcal{D}^* = \frac{\kappa^* \mathcal{L}e}{\rho^* C_{pf}^*} \tag{13}$$

Chemistry Model

An 11-reaction/9-species hydrogen-air chemistry model is employed. The reactions and the corresponding forward reaction rate variables are based on the NASP model[31] and are given in Table 1. The forward reaction rate for the kth reaction is expressed in the following expanded Arrhenius form:

$$K_{f,k}^*(T^*) = AT^{*n} \exp(-\Theta/T^*) \tag{14}$$

In Table 1 the units for the forward reaction rates are cm^3/mole-s or cm^6/mole^2-s and the third-body efficiencies are 2.5 for $M = H_2$, 16.25 for $M = H_2O$ and 1.0 for all other M. The above model of 11 reactions ($m = 11$), 9 species ($n = 9$), and 10 reactants ($n_t = 10$) can be symbolically represented as

Table 1 Reactions and reaction rates

Reaction	A	n	Θ
1) $H + O_2 \rightleftharpoons O + OH$	1.91E + 14	0	8,273
2) $O + H_2 \rightleftharpoons H + OH$	5.06E + 04	2.67	3,166
3) $OH + OH \rightleftharpoons O + H_2O$	1.50E + 09	1.14	0
4) $OH + H_2 \rightleftharpoons H + H_2O$	2.16E + 08	1.51	1,726
5) $O + NO \rightleftharpoons N + O_2$	3.80E + 09	1.0	20,820
6) $O + N_2 \rightleftharpoons NO + N$	1.82E + 14	0	38,370
7) $H + NO \rightleftharpoons N + OH$	1.70E + 14	0	24,560
8) $H + H + M \rightleftharpoons H_2 + M$	7.30E + 17	−1.0	0
9) $H + O + M \rightleftharpoons OH + M$	2.60E + 16	−0.6	0
10) $O + O + M \rightleftharpoons O_2 + M$	1.14E + 17	−1.0	0
11) $H + OH + M \rightleftharpoons H_2O + M$	8.62E + 21	−2.0	0

$$\sum_{l=1}^{n_t} \nu'_{k,l} A_l \rightleftharpoons \sum_{l=1}^{n_t} \nu''_{k,l} A_l, \qquad k = 1, 2, \ldots, m \tag{15}$$

where $\nu'_{k,l}$ and $\nu''_{k,l}$ are the stoichiometric coefficients and A_l is the chemical symbol of the lth species. Using the law of mass action, the mass production/depletion rate of the species s is

$$\begin{aligned} \dot{\omega}_s^* = \mathcal{M}_s^* \sum_{k=1}^{m} (\nu''_{k,s} - \nu'_{k,l}) \Bigg\{ & K_{f,k}^*(T^*) \prod_{r=1}^{n_t} [\rho^* \gamma_r^*]^{\nu'_{k,r}} \\ & - K_{b,k}^*(T^*) \prod_{r=1}^{n_t} [\rho^* \gamma_r^*]^{\nu''_{k,r}} \Bigg\} \end{aligned} \tag{16}$$

The mole-mass ratios of the reactants are defined as

$$\gamma_r^* = \begin{cases} c_r/\mathcal{M}_r^*, & r = 1, 2, \ldots, n \\ \displaystyle\sum_{s=1}^{n} Z_{r,s} \gamma_s^*, & r = n + 1, \ldots, n_t \end{cases} \tag{17}$$

where $Z_{r,s}$ are the third-body efficiencies for each of the species. The backward reaction rate required for $\dot{\omega}_s^*$ is obtained from

$$K_{b,k}^* = \frac{K_{f,k}^*}{K_{\text{eq},k}^*}, \qquad k = 1, 2, \ldots, m \tag{18}$$

where $K_{\text{eq},k}^*$ is the equilibrium constant of the kth reaction given by

$$K_{\text{eq},k}^* = (\mathcal{R}'_U T^*)^{-\Delta n_k} \exp\left(\frac{-\Delta G_k^*}{\mathcal{R}_U T^*}\right) \tag{19}$$

where $\mathcal{R}'_U = 82.06 \times 10^{-6}$ m^3 atm/mole-K,[38] and Δn_k is the integer difference between the numbers of product and reactant species

$$\Delta n_k = \sum_{s=1}^{n} \nu''_{k,s} - \sum_{s=1}^{n} \nu'_{k,s} \tag{20}$$

$$\Delta G_k^* = \sum_{s=1}^{n} \nu''_{k,s} g_s^* - \sum_{s=1}^{n} \nu'_{k,s} g_s^* \tag{21}$$

The species Gibbs free energy g_s are obtained from tables in Ref. 34.

Turbulence Modeling

The algebraic turbulence model proposed by Baldwin and Lomax[39] is used in the present study for turbulent calculations. This model was chosen for its inherent simplicity and for the fact that it gives reasonable results for complex flows with length scales that are not well-defined. For three-dimensional internal corner flows, the turbulence model is modified as proposed by Hung et al.[40] Using the computed eddy viscosities, the thermal conductivity and mass diffusivity are calculated to account for turbulent mixing. A turbulent Prandtl number of 0.9 is used for all the calculations in the present study.

Numerical Method

Gasdynamic Solution

A finite-volume, upwind, TVD scheme is used to integrate the fluid dynamic equations. The algorithm is second-order accurate in the crossflow plane and first-order accurate in the streamwise marching direction. The upwind algorithm is based on Roe's steady approximate Riemann solver[30] which has been modified[20] for nonequilibrium effects. Second-order central differences are used to model the mass diffusion terms and the heat fluxes. Further details of the algorithm can be found in Refs. 27 and 29.

Chemistry Solution

The species continuity equation is solved in a loosely-coupled manner using a finite-volume formulation. The requirement that the mass fractions of the species sum to unity eliminates the nth species continuity equation

$$c_n = 1 - \sum_{s=1}^{n-1} c_s \tag{22}$$

This results in requiring only $n - 1$ equations to be solved. It should be noted that in all the computations performed in this study, N_2 was treated as an inert gas, and hence, was taken as the nth species. The convective terms are modeled using first-order upwind differences and the strong conservation law form is retained by using the fluid fluxes (the coefficients of the convective terms) as known quantities from the most recent fluid integration step. The species production/depletion rate $\dot{\omega}_s$ is treated as a source term and is lagged to the nth marching station for the present calculations.

A line Gauss-Seidel procedure with successive overrelaxation (SOR) is employed. A scalar tridiagonal solver is used to solve the resulting system of equations in an iterative manner until the residual for each of the species drops below a specified tolerance level ε. The residual is defined as

$$|c_s^{i+1} - c_s^i| \leq \varepsilon$$

where $i + 1$ is the current iteration level, and i is the previous iteration level.

Fluid/Chemistry Coupling

The coupling between the fluids and chemistry is achieved in an approximate manner. The fluid step is first taken with frozen chemistry to advance from the n to the $n + 1$ marching station. The fluid density and velocity computed at the new station are then used to advance the chemistry solution to the $n + 1$ level. After determining the species mass fractions, mixture molecular weight, fluid density, and internal energy at the $n + 1$ level, the new pressure, temperature, $\bar{\gamma}$, specific enthalpy, and frozen specific heats are calculated.

The temperature is obtained using the following Newton-Raphson iterative scheme:

$$T^{*k+1} = T^{*k} - \frac{\mathcal{F}(T^{*k}) - e^*}{\mathcal{F}'(T^{*k})} \tag{23}$$

where

$$\mathcal{F}(T^{*k}) = \sum_{s=1}^{n} c_s \left[h_s^*(T^*) - \frac{\mathcal{R}_U T^*}{\mathcal{M}_s^*}\right] \tag{24}$$

$$\mathcal{F}'(T^{*k}) = \sum_{s=1}^{n} c_s \left[C_{p,s}^*(T^*) - \frac{\mathcal{R}_U}{\mathcal{M}_s^*}\right] \tag{25}$$

and k is the iteration level. The iterations are continued until

$$|T^{k+1} - T^k| \leq \delta$$

where δ is a specified tolerance level. The coupling between the fluids and chemistry can be enhanced through the implementation of Newton iterations on the governing equations at each streamwise step.[27]

Numerical Results

The new internal flow UPS code has been used to compute two test cases. The two test cases were chosen to demonstrate and validate the hydrogen-air combustion as well as the three-dimensional internal flow capability of the code. The first test case is the Burrows-Kurkov supersonic combustion experiment,[32] and the second one is a three-dimensional, internal flow, shock-induced combustion case which simulates a generic three-dimensional scramjet flowfield.

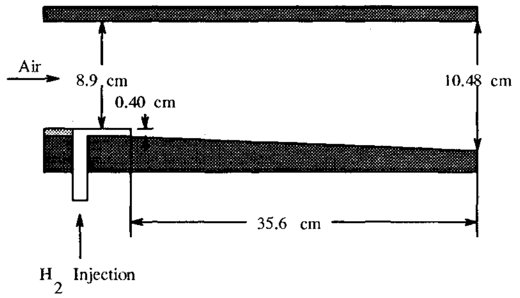

Fig. 1 Schematic of the Burrows-Kurkov experimental setup.

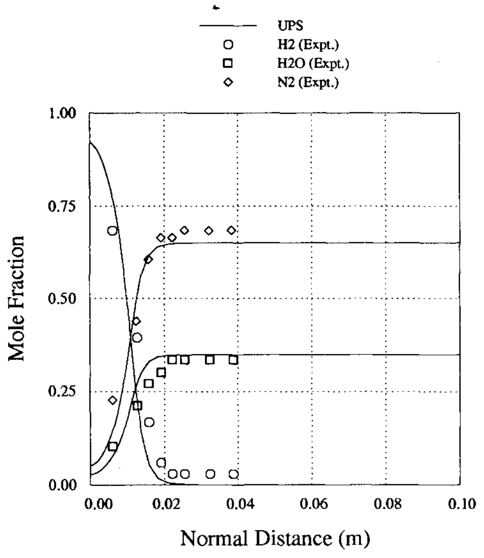

Fig. 2 Species mole fraction profiles at the exit plane (x = 35.6 cm; pure mixing case).

Table 2 Freestream conditions for Burrows-Kurkov experiment

Quantity	H_2 Jet	Vitiated airstream
Mach number	1.0	2.44
Temperature, K	254	1270
Pressure, atm	1.0	1.0
H_2 mass fraction	1.0	0.0
H_2O mass fraction	0.0	0.256
O_2 mass fraction	0.0	0.258
N_2 mass fraction	0.0	0.486

Test Case 1

In the two-dimensional Burrows-Kurkov experiment,[32] combustion occurs in the supersonic shear layer produced by the sonic injection of hydrogen into a stream of vitiated air. The test section consists of two nearly parallel walls with the lower wall slightly angled down. A schematic of the experimental setup is shown in Fig. 1. The freestream conditions for the hydrogen jet and the vitiated air are given in Table 2 and the wall temperature was held constant at 298 K.

For all the calculations, a grid consisting of 101 grid points in the normal direction was used. The grid was clustered near the lower wall in order to properly resolve the shear layer. The first point off the wall was placed at 1.0×10^{-8} m. The Baldwin-Lomax turbulence model was employed to simulate turbulent mixing.

Two computations were performed with the first one being a pure mixing case. In both computations, freestream startup conditions were assumed at the $x = 0$ plane. For the mixing case only, the freestream temperature was set to 1150 K to match the experiment,[32] and all of the O_2 in the vitiated air region was replaced by N_2 so that no combustion takes place. The species mole fraction profiles at the exit plane ($x = 35.6$ cm) are compared with the experimental results in Fig. 2. The computed results are in excellent agreement with the experimental results. The second calculation used the flow conditions listed in Table 2 which allow supersonic combustion to occur. Ignition, based on the mass fraction of OH species, was found to occur at about 15 cm. The species mole fraction profiles at the exit plane are compared with the experimental results in Fig. 3. The flame strength denoted by the peak in the H_2O profile and the mole fraction values at the wall agree well with the experimental predictions. However, all the species profiles are shifted closer to the lower wall. Similar results have been obtained by other investigators[11,22] using the same turbulence model as in this study. A series of grid refinement studies were performed to assess the effect of mesh refinement by varying the number of grid points as well as the grid stretching, and no appreciable change in the behavior of the profiles was found. The total temperature profiles at the exit station are compared in Fig. 4. The computed results, including the peak total temperature location and magnitude, compare well with the experimental data. The CPU time required for the combustion test case was 9.25×10^{-4} s/step/grid point on the CRAY-YMP.

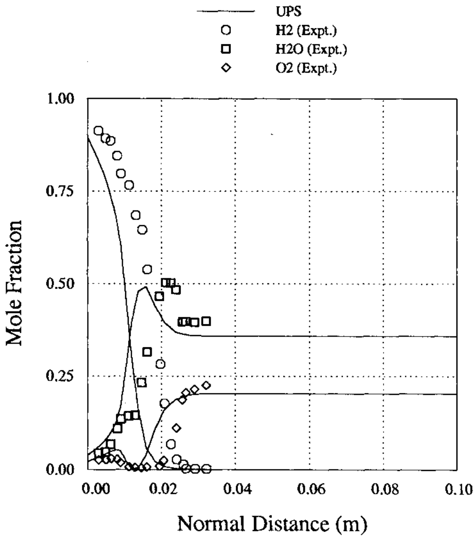

Fig. 3 Species mole fraction profiles at the exit plane ($x = 35.6$ cm; combustion case).

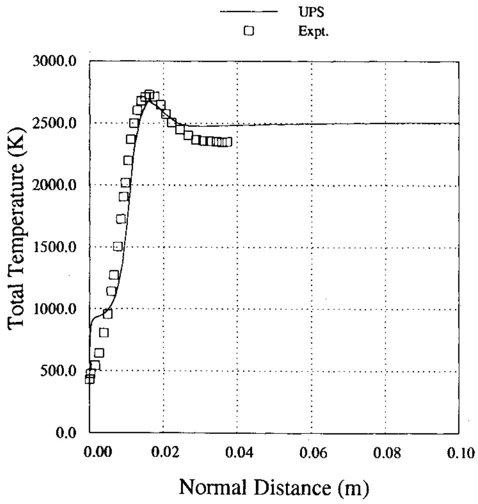

Fig. 4 Total temperature profiles at the exit plane ($x = 35.6$ cm; combustion case).

Test Case 2

The second test case consists of a three-dimensional duct with a 15-deg compression ramp. Air, premixed with hydrogen, enters the duct with a freestream Mach number of 7. Combustion occurs as a result of the shock emanating from the compression ramp. The schematic of the three-dimensional duct is shown in Fig. 5. The side walls have been re-

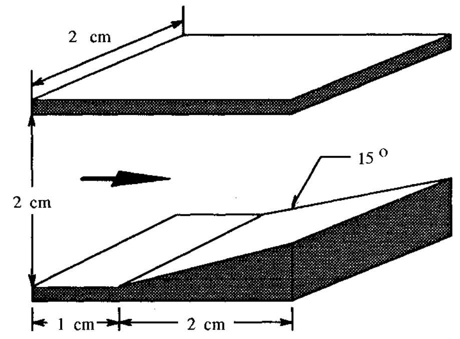

Fig. 5 Schematic of the three-dimensional duct.

Fig. 6 Mach contours in the centerline streamwise plane.

Table 3 Freestream conditions for three-dimensional case

Quantity	Value
Mach number	7.0
Reynolds number, m	1.013×10^6
Temperature, K	1200
H_2 mass fraction	0.03207
O_2 mass fraction	0.25447
N_2 mass fraction	0.71346

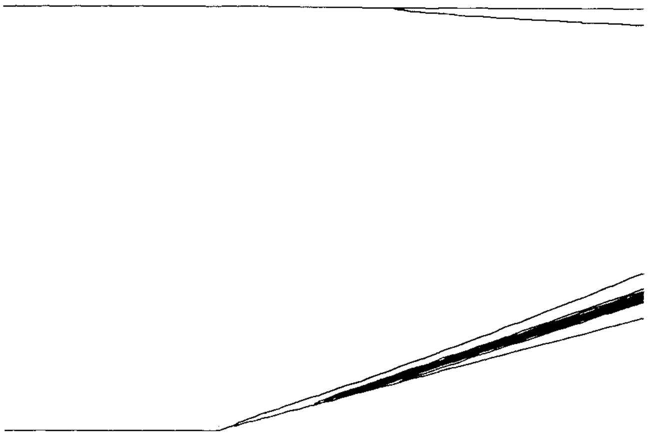

Fig. 7 H_2O mole fraction contours in the centerline streamwise plane.

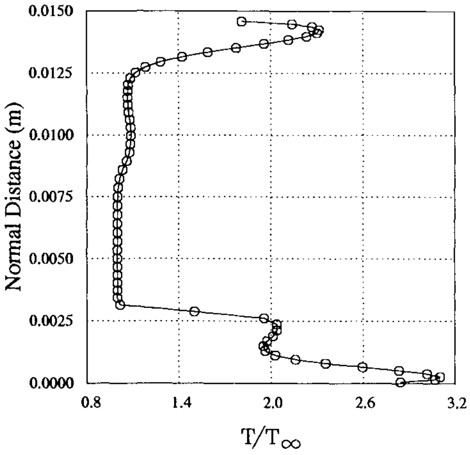

Fig. 8 Temperature profile at centerline of exit plane (x = 3 cm).

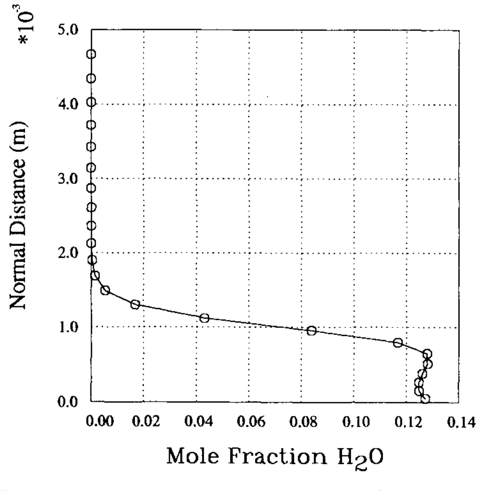

Fig. 9 H_2O mole fraction profile at centerline of exit plane (x = 3 cm).

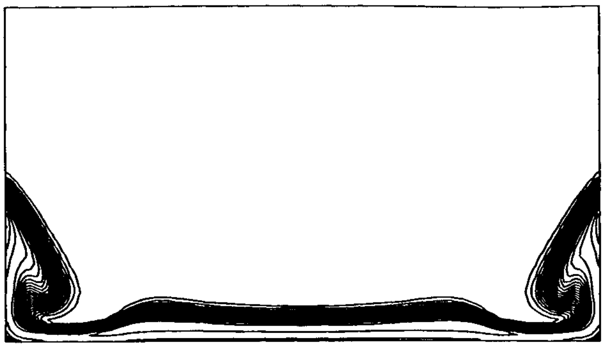

Fig. 10 H_2O mole fraction contours in the crossflow plane at the exit (x = 3 cm).

moved for the sake of clarity. The freestream flow conditions are given in Table 3. The flow is assumed to be turbulent and a constant wall temperature of 500 K is used. A grid consisting of 61 × 61 points at each marching station was clustered at all four walls to properly resolve the boundary layer. Due to the presence of the strong shock, smaller streamwise step sizes were taken in the vicinity of the compression corner.

The contours in the centerline, streamwise plane for Mach number and H_2O mole fraction are shown in Figs. 6 and 7, respectively. As expected, the strong compression shock emanating from the corner induces combustion. The profiles of temperature and H_2O mole fraction at the centerline of the exit plane (x = 3 cm) are shown in Figs. 8 and 9, respectively. The side wall effects can be seen in Fig. 10 which shows the contour plot of the H_2O mole fraction at the exit plane of the test section.

Concluding Remarks

The three-dimensional UPS code has been extended in the present study to solve internal turbulent flows with hydrogen-air chemistry. The code now has the capability to compute external or internal flows with either perfect gas, equilibrium air, nonequilibrium air, or nonequilibrium hydrogen-air chemistry. As a consequence, this code can now be used to compute both aerodynamic and propulsive flowfields associated with hypersonic vehicles such as the NASP.

Acknowledgments

This work was supported by NASA Ames Research Center under Grants NAG 2-502 and NAG 2-776. The technical monitor for these grants is Thomas A. Edwards. The authors thank C. J. Jachimowski, Hypersonic Propulsion Branch, NASA Langley Research Center for information on the thermodynamic data. All the computations in this study were performed on the CCF CRAY-YMP at NASA Ames Research Center.

References

[1] Gnoffo, P. A., and McCandless, R. S., "Three Dimensional AOTV Flowfields in Chemical Nonequilibrium," AIAA Paper 86-0230, Jan. 1986.

[2] Candler, G. V., and MacCormack, R. W., "The Computation of Hypersonic Ionized Flows in Chemical and Thermal Nonequilibrium," AIAA Paper 88-0511, Jan. 1988.

[3] Palaniswamy, S., Chakravarthy, S. R., and Ota, D. K., "Finite-Rate Chemistry for USA—Series Code: Formulation and Applications," AIAA Paper 89-0200, Jan. 1989.

[4] Shuen, J. S., and Liou, M. S., "Flux-Splitting Algorithms for Two-Dimensional Viscous Flows with Finite-Rate Chemistry," AIAA Paper 89-0388, Jan. 1989.

[5] Yu, S. T., Tsai, Y. L. P., and Shuen, J. S., "Three-Dimensional Calculation of Supersonic Reacting Flows Using an LU Scheme," AIAA Paper 89-0391, Jan. 1989.

[6] Palmer, G., "An Efficient, Explicit Finite-Rate Algorithm to Compute Flows in Chemical Nonequilibrium," AIAA Paper 89-0522, Jan. 1989.

[7] Hoffman, J. J., "Development of an Algorithm for the Three-Dimensional Fully-Coupled Navier-Stokes Equations with Finite-Rate Chemistry," AIAA Paper 89-0670, Jan. 1989.

[8] Molvik, G. A., and Merkle, C. L., "A Set of Strongly-Coupled Upwind Algorithms for Computing Flows in Chemical Nonequilibrium," AIAA Paper 89-0199, Jan. 1989.

[9] Imlay, S. T., Roberts, D. W., Soetrisno, M., and Eberhardt, S., "Nonequilibrium Thermo-Chemical Calculations Using a Diagonal Implicit Scheme," AIAA Paper 91-0468, Jan. 1991.

[10] Withington, J. P., Shuen, J. S., and Yang, V., "A Time Accurate Implicit Method for Chemically Reacting Flows at All Mach Numbers," AIAA Paper 91-0581, Jan. 1991.

[11] Walters, R. W., Cinnella, P., Slack, D. C., and Halt, D., "Characteristic Based Algorithms for Flows in Thermochemical Non-Equi-

librium," *AIAA Journal*, Vol. 30, No. 5, 1992, pp. 1304–1313.

[12]Bhutta, B. A., Lewis, C. H., and Kautz, F. A., II, "A Fast Fully-Iterative Parabolized Navier-Stokes Scheme for Chemically-Reacting Reentry Flows," AIAA Paper 85-0926, June 1985.

[13]Bhutta, B. A., and Lewis, C. H., "Three Dimensional Hypersonic Nonequilibrium Flows at Large Angles of Attack," *Journal of Spacecraft and Rockets*, Vol. 26, No. 3, 1989, pp. 158–166.

[14]Prabhu, D. K., Tannehill, J. C., and Marvin, J. G., "A New PNS Code for Chemical Nonequilibrium Flows," *AIAA Journal*, Vol. 26, No. 7, 1988, pp. 808–815.

[15]Prabhu, D. K., Tannehill, J. C., and Marvin, J. G., "A New PNS Code for Three-Dimensional Chemically Reacting Flows," *Journal of Thermophysics and Heat Transfer*, Vol. 4, No. 3, 1990, pp. 257, 258.

[16]Sinha, N., Dash, S. M., and Krawczyk, W. J., "Inclusion of Chemical Kinetics into Beam-Warming Based PNS Model for Hypersonic Propulsion Applications," AIAA Paper 87-1898, June 1987.

[17]Korte, J. J., and McRae, D. S., "Explicit Upwind Algorithm for the Parabolized Navier-Stokes Equations," AIAA Paper 88-0716, Jan. 1988.

[18]Chitsomboon, T., and Northam, G. B., "A 3D-PNS Computer Code for the Calculation of Supersonic Combusting Flows," AIAA Paper 88-0438, Jan. 1988.

[19]Tannehill, J. C., Ievalts, J. O., and Lawrence, S. L., "An Upwind Parabolized Navier-Stokes Code for Real Gas Flows," AIAA Paper 88-0713, Jan. 1988.

[20]Tannehill, J. C., Ievalts, J. O., Buelow, P. E., Prabhu, D. K., and Lawrence, S. L., "Upwind Parabolized Navier-Stokes Code for Chemically Reacting Flows," *Journal of Thermophysics and Heat Transfer*, Vol. 4, No. 2, 1990, pp. 149–156.

[21]Gielda, T., and Agarwal, R., "Efficient Finite-Volume Parabolized Navier-Stokes Solutions for Three-Dimensional, Hypersonic, Chemically Reacting Flowfields," AIAA Paper 89-0103, Jan. 1989.

[22]Kamath, H., "Parabolized Navier-Stokes Algorithm for Chemically Reacting Flows," AIAA Paper 89-0386, Jan. 1989.

[23]Liou, M. F., "Three Dimensional PNS Solutions of Hypersonic Internal Flows with Equilibrium Chemistry," AIAA Paper 89-0002, Jan. 1989.

[24]Sinha, N., Dash, S. M., and Lee, R. A., "3-D PNS Analysis of Scramjet Combustion/Nozzle and Exhaust Plume Flowfields," AIAA Paper 90-0094, Jan. 1990.

[25]Tannehill, J. C., Buelow, P. E., Ievalts, J. O., and Lawrence, S. L., "Three-Dimensional Upwind Parabolized Navier-Stokes Code for Real Gas Flows," *Journal of Spacecraft and Rockets*, Vol. 27, No. 2, 1990, pp. 150–159.

[26]Gerbsch, R. A., and Agarwal, R. K., "Solution of the Parabolized Navier-Stokes Equations for Three-Dimensional Real-Gas Flows Using Osher's Upwind Scheme," AIAA Paper 91-0248, Jan. 1991.

[27]Buelow, P. E., Tannehill, J. C., Ievalts, J. O., and Lawrence, S. L., "A Three-Dimensional, Upwind, Parabolized Navier-Stokes Code for Chemically Reacting Flows," *Journal of Thermophysics and Heat Transfer*, Vol. 5, No. 3, 1991, pp. 274–283.

[28]Lawrence, S. L., Tannehill, J. C., and Chaussee, D. S., "Upwind Algorithm for the Parabolized Navier-Stokes Equations," *AIAA Journal*, Vol. 27, No. 9, 1989, pp. 1175–1183.

[29]Lawrence, S. L., Chaussee, D. S., and Tannehill, J. C., "Application of an Upwind Algorithm to the Three-Dimensional Parabolized Navier-Stokes Equations," *AIAA Journal*, Vol. 28, No. 6, 1990, pp. 971, 972.

[30]Roe, P. L., "Approximate Riemann Solvers, Parameter Vectors, and Difference Schemes," *Journal of Computational Physics*, Vol. 43, No. 2, 1981, pp. 357–372.

[31]Oldenborg, R., Chinitz, W., Friedman, M., Jaffe, R., Jachimowski, C., Rabinowitz, M., and Schott, G., "Hypersonic Combustion Kinetics: Status Report of Rate Constant Committee, NASP High-Speed Propulsion Technology Team," NASP TM-1107, May 1990.

[32]Burrows, M. C., and Kurkov, A. P., "Analytical and Experimental Study of Supersonic Combustion of Hydrogen in a Vitiated Airstream," NASA TM X-2828, Sept. 1973.

[33]Vigneron, Y. C., Rakich, J. V., and Tannehill, J. C., "Calculation of Supersonic Flow over Delta Wings with Sharp Subsonic Leading Edges," AIAA Paper 78-1137, July 1978.

[34]McBride, B. J., Heimel, S., Ehlers, J. G., and Gordon, S., "Thermodynamic Properties to 6000° K for 210 Substances Involving the First 18 Elements," NASA SP-3001, 1963.

[35]Svehla, R. A., "Estimated Viscosities and Thermal Conductivities of Gases at High Temperatures," NASA TR R-132, 1962.

[36]Wilke, C. R., "A Viscosity Equation for Gas Mixtures," *Journal of Chemical Physics*, Vol. 18, No. 4, 1950, p. 517–519.

[37]Strehlow, R. A., *Combustion Fundamentals*, McGraw-Hill, New York, 1984.

[38]Gardiner, W. C., Jr., *Combustion Chemistry*, Springer-Verlag, New York, 1984.

[39]Baldwin, B. S., and Lomax, H., "Thin Layer Approximation and Algebraic Model for Separated Turbulent Flows," AIAA Paper 78-257, Jan. 1978.

[40]Hung, C.-M., and Buning, P. G., "Simulation of Blunt-Fin-Induced Shock-Wave and Turbulent Boundary-Layer Interaction," *Journal of Fluid Mechanics*, Vol. 154, 1985, pp. 163–185.